Macroscopic phase-resetting curves for spiking neural networks

Grégory Dumont*
Group for Neural Theory, LNC INSERM U960, DEC, Ecole Normale Superieure PSL University, 75005 Paris France*

G. Bard Ermentrout
Department of Mathematics, University of Pittsburgh, 15260 Pittsburgh, Pennsylvania, USA

Boris Gutkin
Group for Neural Theory, LNC INSERM U960, DEC, Ecole Normale Superieure PSL University, 75005 Paris France*
and Center for Cognition and Decision Making, Department of Psychology, NRU Higher School of Economics, 101000 Moscow, Russia
(Received 1 August 2017; published 30 October 2017)

The study of brain rhythms is an open-ended, and challenging, subject of interest in neuroscience. One of the best tools for the understanding of oscillations at the *single neuron* level is the phase-resetting curve (PRC). Synchronization in networks of neurons, effects of noise on the rhythms, effects of transient stimuli on the ongoing rhythmic activity, and many other features can be understood by the PRC. However, most macroscopic brain rhythms are generated by large *populations* of neurons, and so far it has been unclear how the PRC formulation can be extended to these more common rhythms. In this paper, we describe a framework to determine a macroscopic PRC (mPRC) for a network of spiking excitatory and inhibitory neurons that generate a macroscopic rhythm. We take advantage of a thermodynamic approach combined with a reduction method to simplify the network description to a small number of ordinary differential equations. From this simplified but exact reduction, we can compute the mPRC via the standard adjoint method. Our theoretical findings are illustrated with and supported by numerical simulations of the full spiking network. Notably our mPRC framework allows us to predict the difference between effects of transient inputs to the excitatory versus the inhibitory neurons in the network.

DOI: 10.1103/PhysRevE.96.042311

I. INTRODUCTION

Emerging oscillations are ubiquitous in nature [1,2]; brain rhythms, for example, form a basis for multiple cognitive functions [3]. Within the dynamical systems framework, such rhythms can be seen as limit cycles, and like the limit cycles of single neuron oscillations, these rhythms have a phase-resetting curve (PRC) [2], a function that describes how the oscillation shifts depending on the timing or phase of the input. The PRC can be computed directly (e.g., by simulation or experimentally) for any rhythm by applying short pulses at different phases of the cycle and observing the phase shift. The PRC method and its benefits, such as the mechanistic understanding of neural synchronization, have been reviewed by various authors [4–6]. Of course, similar outcomes are expected for brain rhythms [7].

For oscillations defined by a dynamical system, such as many coupled differential equations, it is much easier and more accurate to compute the infinitesimal PRC (iPRC) by solving a certain linear equation. In the case of single neuron models, this is quite easy to do numerically and even, in some cases, analytically [8]. A major theoretical challenge has been to provide analytical derivations of iPRCs for macroscopic oscillations [9,10]. Yet despite extensive research, computing the iPRC of a conductance-based spiking neural network exhibiting emergent population-wide oscillations has remained an open issue (yet see Ref. [11] for a step in that direction). Recently, the adjoint method, which is at the core of the iPRC computation (see Ref. [8]), has been generalized in a number of ways: for Fokker-Planck equations [11], delay differential equations [12], and reaction diffusion systems [13].

In this paper, we develop a framework to determine a macroscopic phase response curve (mPRC) for spiking networks with heterogeneous neural populations. To do so we take advantage of a thermodynamic approach combined with the reduction method developed by Montbrió, Pazó, and Roxin (MPR) [14]. The mean-field framework produces an analytically tractable population model written in terms of partial differential equations (PDEs), which gives access to the firing activity of the network [15]. The MPR reduction allows further simplification and breaks down the PDE into a low-dimensional system. Such a reduced description can be related, via a conformal map, with the low-dimensional description in terms of the Kuramoto order parameter provided by the Ott-Antonsen theory [16] and recently applied in neuroscience [17]. However, the MPR reduction has the advantage to be written in terms of a dynamical system involving the firing activity and the mean membrane potential of the network, two quantities of interest in neuroscience.

Applying the MPR reduction, we simplify the description of an excitatory-inhibitory neural network. Bifurcation analysis of the reduced system enables us to reveal how synaptic interactions and inhibitory feedback permit the emergence of the macroscopic rhythms. The resulting low-dimensional system allows us to easily apply the usual adjoint method and obtain an expression for the macroscopic iPRC.

The paper is structured as follows. First, we present the network and our neuron model of choice which will be used throughout. Then we go over the MPR reduction and the

Group for Neural Theory, LNC INSERM U960, DEC, Ecole Normale Superieure PSL University, Paris France; gregory.dumont@ens.fr

low-dimensional system for which we perform a bifurcation analysis and extract the infinitesimal PRC. We support our findings with extensive numerical evidence involving simulation of finite-size networks neurons compared with the reduced system.

II. THE NETWORK AND ITS REDUCED SYSTEM

The circuit considered is a network of N_e excitatory cells (E cells) and N_i inhibitory cells (I cells) all-to-all connected with delta-pulse synapses. Each cell is characterized by the quadratic integrate-and-fire (QIF), a well-established model that describes the dynamics, subthreshold, and spike generating, of the neural membrane potential [18,19]. The QIF model is endowed with a discontinuous reset that models the depolarization and the relative refractory period after an action potential. When the voltage reaches a cut off value v_{th}, considered to be the peak of a spike, it is reset to v_r, a reset parameter. In this study, to facilitate analysis, threshold v_{th} and reset v_r are, respectively, set at positive and negative infinity [18]. The QIF reads

$$\tau \frac{d}{dt} v_j(t) = \eta_j + v_j^2(t) + I(t), \tag{1}$$

where $v(t)$ is the membrane potential, τ the membrane time constant, η the bias current that defines the intrinsic resting potential and firing threshold of the cell (see Ref. [18] for more details), and $I(t)$ the total synaptic current injected at the soma. To account for the network heterogeneity, the intrinsic parameter η is distributed randomly according to a Lorentzian distribution:

$$\mathcal{L}(\eta) = \frac{1}{\pi} \frac{\Delta}{(\eta - \bar{\eta})^2 + \Delta^2}.$$

Here $\bar{\eta}$ stands for the mean value taken by the parameter η across the population, and Δ is the half-width of the distribution. The total synaptic current, $I(t)$, depends on the cell type. For the E cells, respectively for the I cells, we have

$$I_e(t) = I_e^{\text{ext}}(t) + J_{ee}\tau_e r_e - J_{ei}\tau_e r_i,$$
$$I_i(t) = I_i^{\text{ext}}(t) + J_{ie}\tau_i r_e - J_{ii}\tau_i r_i.$$

Here I^{ext} is an external current, J the synaptic strength, and $r(t)$ the population firing rate:

$$r_e(t) = \frac{1}{N_e} \sum_{k=1}^{N_e} \sum_f \delta\big(t - t_f^k\big), \quad r_i(t) = \frac{1}{N_i} \sum_{k=1}^{N_i} \sum_f \delta\big(t - t_f^k\big),$$

where δ is the Dirac mass measure and t_f^k the firing time of the neuron numbered k.

In the mean-field limit (see, e.g., Ref. [15]) the system is well represented by the probability of finding the membrane potential of any randomly chosen neuron at voltage v at time t knowing that its intrinsic parameter is η. The dynamic evolution of this density, which we denote $p_e(t,v|\eta)$ for the E cells and $p_i(t,v|\eta)$ for the I cells, is given by a continuous transport equation written in the form of a conservation law (see Appendixes A–C for more details):

$$\tau \frac{\partial}{\partial t} p(t,v|\eta) + \frac{\partial}{\partial v} \mathfrak{J}(t,v|\eta) = 0, \tag{2}$$

where the total probability flux is defined as

$$\mathcal{J}(t,v|\eta) = [\eta + v^2 + I(t)]p(t,v|\eta).$$

A boundary condition for the flux, consistent with the reset mechanism of the QIF model (1), is imposed:

$$\lim_{v\to-\infty} \mathcal{J}(t,v|\eta) = \lim_{v\to+\infty} \mathcal{J}(t,v|\eta).$$

The firing rate of the considered population $r(t)$ is given by the flux through the threshold:

$$r(t) = \lim_{v\to+\infty} \int_{-\infty}^{+\infty} \mathcal{L}(\eta)\mathcal{J}(t,v|\eta)\, d\eta.$$

One can show that [14] the PDE (2) reduces to a low-dimensional dynamical system. In our case (see Appendix C for more details) the dynamics of the two coupled PDEs that describe the time evolution of $p_e(t,v|\eta)$ and $p_i(t,v|\eta)$ reduces to a set of four differential equations,

$$\begin{aligned} \tau_e \frac{d}{dt} r_e &= \frac{\Delta_e}{\pi\tau_e} + 2\pi r_e V_e \\ \tau_e \frac{d}{dt} V_e &= V_e^2 + \bar{\eta}_e + I_e(t) - \pi^2 r_e^2, \end{aligned} \tag{3}$$

and for the I cells,

$$\begin{aligned} \tau_i \frac{d}{dt} r_i &= \frac{\Delta_i}{\pi\tau_i} + 2\pi r_i V_i \\ \tau_i \frac{d}{dt} V_i &= V_i^2 + \bar{\eta}_i + I_i(t) - \pi^2 r_i^2, \end{aligned} \tag{4}$$

where $V(t)$ represents the mean potential of the population:

$$V(t) = \int_{-\infty}^{+\infty} \mathcal{L}(\eta) \int_{-\infty}^{+\infty} v p(t,v|\eta)\, dv\, d\eta.$$

Note that the second integral is defined via the Cauchy principal value, the reason being that the Lorentz distribution only has a mean in the principal value sense; see Appendix B. Note also that in this reduced formulation, the two subsystems are coupled and the coupling is made via their respective total synaptic currents $I_e(t)$; $I_i(t)$.

The numerical simulation presented in Fig. 1 illustrates a comparison between the dynamics of the full network and the low-dimensional system (3)–(4). It shows the time evolution of the external stimulus in the first panel [Fig. 1(a)], whereas the second panel gives the spiking activity obtained from a simulation of the full network [Fig. 1(b)]. In the subsequent panels [Figs. 1(c)–1(d)], the firing rate given by the reduced description is compared with the firing rate obtained from network simulations. The blue line corresponds to the I cells, and the red line to the E cells. The reduced description captures the essential shape of the firing activity of the full network, and, of course, it has the advantage to be low dimensional. The perfect agreement confirms the validity of the reduction.

Note that the reduced dynamical system (3)–(4) shares some similarities with the Wilson-Cowan model [20]. Bifurcation analysis reveals that the low-dimensional system (3)–(4) exhibits a Hopf bifurcation as the E drive is increased [see Fig. 2(a)]; this rhythmic regime disappears as the heterogeneity (Δ) in the network is increased [see Fig. 2(b)]. We see from the network raster plots [Fig. 2(d)] that both the E and I cell

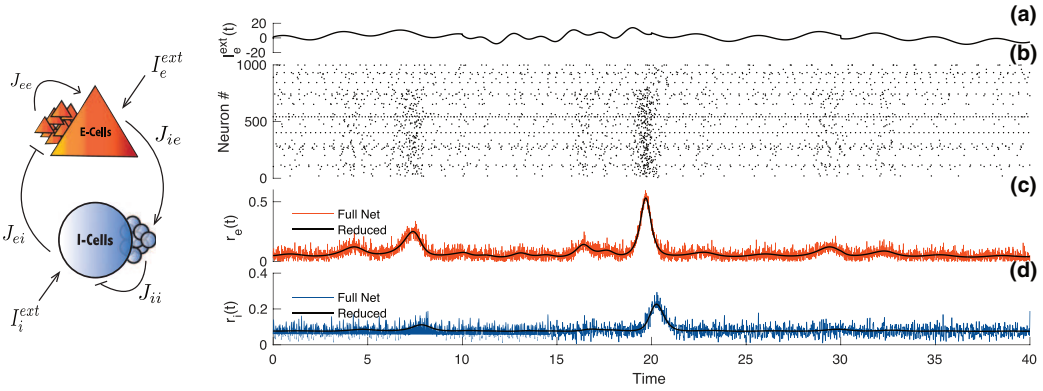

FIG. 1. Comparison between the full network dynamics and the reduced system. Left panel: Schematic illustration of the neural network. The parameter $J_{\alpha\beta}$ denotes the connectivity strength of the population β onto the population α. The external influence on the population α is denoted $I_\alpha^{\rm ext}$. Right panels: Comparison. (a) Time evolution of the stimulus $I_e^{\rm ext}$ on the E cells. (b) Spiking activity obtained from simulations of the full network; the first 800 cells are excitatory, the last 200 are inhibitory. (c) Firing rate of the E cells obtained from simulations of the full network (red line) compared with the reduced system (black line). (d) Firing rate of the I cells obtained from simulations of the full network (blue line) compared with the reduced system (black line). Parameters: $N_e = N_i = 5000$; $\Delta_e = \Delta_i = 1$; $\tau_e = \tau_i = 1$; $\bar\eta_e = \bar\eta_i = -5$; $J_{ee} = 0$; $J_{ei} = 15$; $J_{ii} = 0$; $J_{ie} = 15$; $I_i^{\rm ext} = 0$; $v_{th} = 200$; $v_r = -200$.

populations globally engage in rhythmic behavior as soon as the external E drive is sufficiently strong [Fig. 2(c)].

The mechanism underlying this macroscopic oscillation is known as the PING (Pyramidal Interneuron Network Gamma) interaction [21]. We note that since by design the neurons within the network are parametrically heterogenous, with a portion of them not being excitable (as opposed to oscillators), the rhythm emerges at the global network scale. In other words, if we were to disconnect the network, no oscillatory rhythm would be observable.

III. PHASE-RESETTING CURVE

Being applicable to every self-sustained oscillatory system, PRC has turned into an essential measure in nonlinear science. It quantifies the effect of external perturbation on stable limit cycles. When a short depolarizing current is applied to the network, the spiking activity and resulting macroscopic oscillation will shift in time. We can choose to apply the short depolarizing input to the excitatory or the inhibitory neurons. Raster plots from numerical simulations of the full network [Fig. 3(a)] illustrate the shift. Here the black dots correspond to the unperturbed network, and the colored dots to the perturbed circuit. Before the stimulus onset [Fig. 3(b)], the two rasters overlap perfectly. After the stimulus presentation, spikes of the perturbed network are shifted: either delayed [Fig. 3(a)] or advanced [Fig. 3(b)] depending on the onset phase of the perturbation. The mPRC results in plotting the advance or delay as a function of the perturbation phase onset [Figs. 4(a)–4(b)].

The iPRC is defined mathematically for infinitesimally small perturbation, and it is computed in a perfectly rigorous

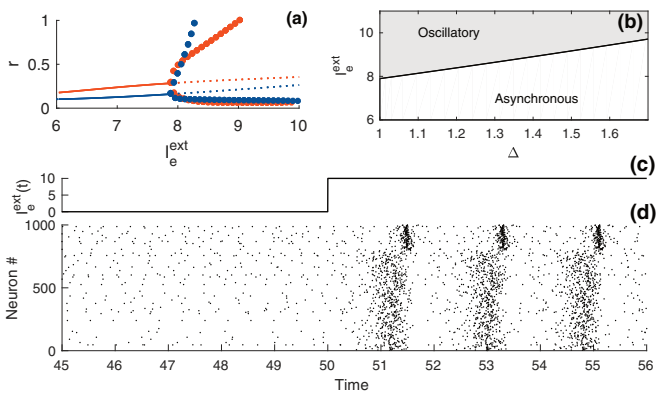

FIG. 2. Bifurcation diagram. (a) The blue line (respectively, the red line) corresponds to the steady state of the inhibitory cells (respectively the excitatory cells), and dots correspond to limit cycles. (b) Stability region. (c) Illustration of the stimulus. (d) Raster plot of the spiking activity. The parameters are the same as in Fig. 1.

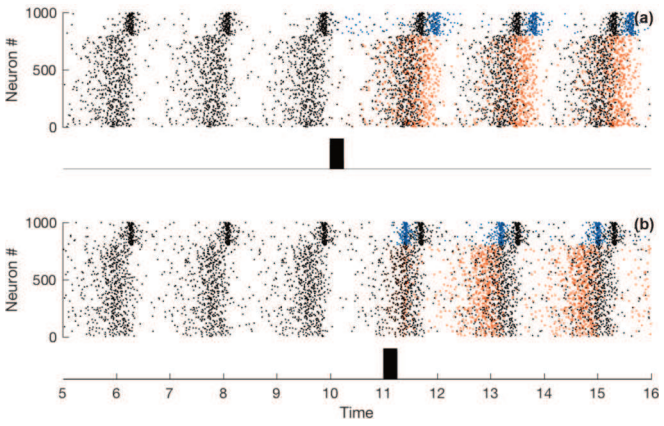

FIG. 3. Illustration of stimulus-induced phase shifting. (a), (b) Top panels: Spiking activity obtained from simulations of the full spiking network. The black dots illustrate the ongoing activity and the colored dots (blue for the I cells and red for the E cells) the activity of the perturbed network. Lower panels: Illustration of the stimulus. For this example, the perturbation is made with a square wave current pulse (amplitude 20, duration 0.25) to the I cells. The network parameters are the same as in Fig. 1 with $I_e^{\rm ext} = 10$.

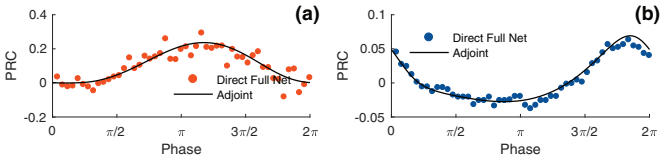

FIG. 4. Comparison between simulated and calculated mPRCs. The black line illustrates the analytical adjoint method, and dots indicates direct perturbations of the full spiking neural network. (a) The perturbation is delivered to the E cells. (b) The perturbation is delivered to the I cells. The network parameters are the same as in Fig. 1 with $I_e^{\text{ext}} = 10$, the perturbation made with a square wave current pulse (amplitude 10, duration 0.05).

way via the adjoint method [8]. This method can be applied on the low-dimensional system (3)–(4), and a semianalytical expression of the infinitesimal mPRC can be extracted; see Appendix D. Assuming that

$$O(t) = (r_{e_o}(t), V_{e_o}(t), r_{i_o}(t), V_{i_o}(t)),$$

is a stable limit cycle of the E-I system (3)–(4) of period T, that is,

$$O(t) = O(t+T),$$

we find that the iPRC $Z(t)$ is a periodic vector of four components,

$$Z(t) = (Z_{r_e}(t), Z_{v_e}(t), Z_{r_i}(t), Z_{v_i}(t)),$$

that is a solution of the adjoint equation

$$-\frac{d}{dt}Z(t) = \mathcal{M}(t)^T \cdot Z(t), \tag{5}$$

where the matrix $\mathcal{M}(t)$ is given by a linearization of the E-I system (3)–(4) around the limit cycle:

$$\mathcal{M}(t) = \begin{bmatrix} \frac{2V_{e_o}(t)}{\tau_e} & \frac{2r_{e_o}(t)}{\tau_e} & 0 & 0 \\ -2\tau_e\pi^2 r_{e_o}(t) + J_{ee} & \frac{2V_{e_o}(t)}{\tau_e} & -J_{ei} & 0 \\ 0 & 0 & \frac{2V_{i_o}(t)}{\tau_i} & \frac{2r_{i_o}(t)}{\tau_i} \\ J_{ie} & 0 & -2\tau_i\pi^2 r_{i_o}(t) - J_{ii} & \frac{2V_{i_o}(t)}{\tau_i} \end{bmatrix}.$$

The iPRC $Z(t)$ is given by the unique periodic solution that satisfies the normalization condition

$$Z(t) \cdot \dot{O}(t) = 2\pi/T.$$

When perturbations made to the network are small enough, the iPRC will be proportional to the mPRC [11–13].

When we compare the analytically determined infinitesimal mPRC (5) to the mPRC obtained from direct perturbations of the spiking neural network (Fig. 4), it shows an excellent agreement, confirming the validity of the theoretical approach. The two panels correspond to perturbations made onto the membrane voltage of the E cells [Fig. 4(a)] and the I cells [Fig. 4(b)]. We carried out comparisons for simulations with a wide range of network parameters with good agreement. We note, of course, that modifying the network parameters, such as the external drive I_e^{ext}, will affect the shape of the mPRC; see Fig. 5.

Note the biphasic shape of the mPRC [see Fig. 4(b) or Fig. 5(b)] when perturbations are made on the I cells. In contrast, when perturbations are on the E cells, the mPRC is monophasic [see Fig. 4(a) or Fig. 5(a)]. We also note that for this set of parameters, the network is more sensitive to perturbation to the excitatory cells than to the inhibitory cells as is clear from the difference in amplitudes of the respective mPRCs. We observe that modification of network parameters mostly impacts the amplitude of the PRC. Indeed, as we shall see in Fig. 5, the PRC amplitude becomes much smaller when increasing the coupling strength. This can be intuitively interpreted as an increase of robustness of the macroscopic oscillation against external perturbations.

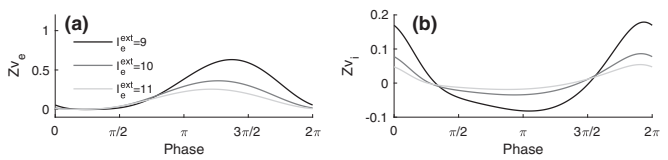

FIG. 5. PRC shape in function of parameters. (a) PRC Z_{v_i} obtained via the adjoint method. (b) PRC Z_{v_e} obtained via the adjoint method. The network parameters are the same as in Fig. 1.

IV. CONCLUSION

The PRC framework is among the most influential of neuroscience theories. It has already generated key insights, including an appreciation for the emergence of neural synchronization [22,23]. The need for this conceptual tool to investigate brain rhythms is underscored by the fact that PRC can provide clarity into their informational properties [7]. Important strides are being taken in that direction, and a number of efforts have been taken to compute the iPRC of emerging macroscopic oscillations in spiking networks [11].

In this study, we developed methodology to compute macroscopic iPRCs for emergent network oscillations using recent framework for analytically tractable reduction of large spiking networks [14–17]. By contrast to previous works (see, e.g., Ref. [11]) where the analytical derivation of the mPRC relies on the computation of the dual system of a partial differential equation, our derivation is made via the usual adjoint method.

Although we have restrained ourselves to considering networks with homogenous synaptic weights, the framework is sufficiently flexible to allow a certain level of synaptic heterogeneity [14]. Another restriction made here is the absence of conduction delays within the local circuit. Again,

a generalization to include the delays poses no problem since the low-dimensional reduction can be achieved with delay [24], and the adjoint method still applies for delay differential equations [12]. We note that it is unclear how existing methods to compute mPRCs for a population of oscillators [10,25] generalize in this situation.

We further note that the framework developed in Refs. [10,25] assumes that the interaction across oscillators is made via a sine wave coupling function. Although it can be appropriate in a variety of biological contexts, it is simply unrealistic for neural circuits. The description of synaptic interaction within the Kuramoto framework is built upon the expression of the interaction function [4]. The interaction function describes the effect of the coupling onto the phase of the neural oscillator. Unfortunately, it is far from being a sine wave, and its general form does not permit the use of the Ott-Antonsen reduction as it is needed in Refs. [10,25]. Therefore, whereas the method described by Refs. [10,25] permits us to link the PRC of the individual units to the mPRC, it is unfortunately not very well suited for the computation of the mPRC of neural networks.

The main limitation is that our derivation is built upon the work of Ref. [14]. As a consequence, our strategy can be applied only to neural network made up of individual units described by the QIF model. It does not apply for a network of leaky integrate-and-fire neurons, for instance.

As we have seen, our analytical computations enable us to make key predictions about the origin of biphasic versus monophasic PRCs. In the light of our theory, the biphasic PRC observed in neural networks can be interpreted as arising from stimulation targeting the inhibitory neurons; on the other hand, the monophasic PRC is characteristic of stimulation onto the excitatory cells. Biphasic PRCs are known to facilitate entrainment to periodic inputs at both higher and lower frequencies than the natural frequency of the network. This provides some theoretical supports for the strong implication of interneurons not only on the emergence of macroscopic oscillations, but also on locking capacity of neural networks [26,27].

Our work also opens new avenues to study the links between the biophysics of the neurons, network connectivity, and the time-persistent phase relationships seen during *in vivo* brain activity and that have been proposed to play a crucial role in the transfer and control of information across brain regions [28]. Thus, the proposed method could be a key technique to elucidate the underlying synaptic mechanism and the functional roles of the so-called cross frequency coupling observed in theta-gamma oscillations, for instance [29].

ACKNOWLEDGMENTS

This study was funded by CNRS, INSERM, and partial support from LABEX ANR-10-LABX-0087 IEC and IDEX ANR-10-IDEX-0001-02 PSL*. The study received support from the Russian Science Foundation grant (Contract No. 17-11-01273).

APPENDIX A: MEAN-FIELD DESCRIPTION

In the mean-field limit (see, e.g., Ref. [15]) the system is well represented by the probability of finding the membrane potential of any randomly chosen neuron at voltage v at time t knowing that its intrinsic parameter is η. The dynamics of this density, which we denote $p(t,v|\eta)$, is given by a continuous transport equation written in the form of a conservation law:

$$\tau \frac{\partial}{\partial t} p(t,v|\eta) + \frac{\partial}{\partial v} \mathfrak{J}(t,v|\eta) = 0, \tag{A1}$$

where the total probability flux is defined as

$$\mathcal{J}(t,v|\eta) = [\eta + v^2 + I(t)] p(t,v|\eta).$$

A boundary condition for the flux, consistent with the reset mechanism of the QIF model, is imposed:

$$\lim_{v\to-\infty} \mathcal{J}(t,v|\eta) = \lim_{v\to+\infty} \mathcal{J}(t,v|\eta).$$

Due to the boundary condition, one can check easily the conservation property of the equation:

$$\int_{-\infty}^{+\infty} p(t,v|\eta)\, dv = \mathcal{L}(\eta),$$

with $\mathcal{L}$ the Lorentzian distribution,

$$\mathcal{L}(\eta) = \frac{1}{\pi} \frac{\Delta}{(\eta - \bar{\eta})^2 + \Delta^2},$$

that defines the probability that a cell has an intrinsic parameter η. The firing rate of the population $r(t)$ is the flux through the threshold, defining

$$r(t,\eta) = \lim_{v\to+\infty} \mathcal{J}(t,v|\eta);$$

the total firing rate is then

$$r(t) = \lim_{v\to+\infty} \int_{-\infty}^{+\infty} \mathcal{L}(\eta) \mathcal{J}(t,v|\eta)\, d\eta.$$

APPENDIX B: REDUCTION

The reduction [14] consists of assuming that the solution of the partial differential equation (A1) has the form of a Lorentzian distribution:

$$p(t,v|\eta) = \frac{1}{\pi} \frac{x(t,\eta)}{[v - y(t,\eta)]^2 + x(t,\eta)^2}. \tag{B1}$$

The mean potential and the firing rate are related to the Lorentzian coefficients:

$$r(t,\eta) = \frac{1}{\pi} x(t,\eta)$$

and

$$y(t,\eta) = \int_{-\infty}^{+\infty} v p(t,v|\eta)\, dv,$$

so in the end, the mean membrane potential is defined as

$$V(t) = \lim_{M\to+\infty} \int_{-M}^{+M} \mathcal{L}(\eta) y(t,\eta)\, d\eta.$$

After algebraic manipulation [14], the transport equation (A1) reduces to the low-dimensional dynamical system

$$\tau \frac{d}{dt} r = \frac{\Delta}{\pi\tau} + 2\pi r V$$

$$\tau \frac{d}{dt} V = V^2 + \bar{\eta} + I(t) - \pi^2 r^2.$$

APPENDIX C: E-I INTERACTION SYSTEM

1. Mean-field description

Considering now a network of two interacting neural populations, the system is then represented by two probability density functions, one for the excitatory neurons, which we denote $p_e(t,v|\eta_e)$, and one for the inhibitory cells, $p_i(t,v|\eta_i)$. Each density follows a continuous transport equation; for the E cells we have

$$\tau_e \frac{\partial}{\partial t} p_e(t,v|\eta_e) + \frac{\partial}{\partial v} \mathfrak{J}_e(t,v|\eta_e) = 0, \tag{C1}$$

where the total probability flux is defined as

$$\mathcal{J}_e(t,v|\eta_e) = [\eta_e + v^2 + I_e(t)] p_e(t,v|\eta_e).$$

A boundary condition for the flux, consistent with the reset mechanism of the QIF model, is imposed. The firing rate of the population $r(t)$ is the flux through the threshold. Having set the threshold at infinity, we get

$$r_e(t,\eta_e) = \lim_{v\to+\infty} \mathcal{J}_e(t,v|\eta_e),$$

and thus the total firing rate

$$r_e(t) = \int_{-\infty}^{+\infty} \mathcal{L}_e(\eta_e) r(t,\eta_e)\, d\eta_e,$$

where $\mathcal{L}_e$ is the Lorentzian distribution,

$$\mathcal{L}_e(\eta_e) = \frac{1}{\pi} \frac{\Delta_e}{(\eta_e - \bar{\eta_e})^2 + \Delta_e^2},$$

that defines the probability that a randomly chosen E cell has an intrinsic parameter η_e. Similarly for the I cells, we have

$$\tau_i \frac{\partial}{\partial t} p_i(t,v|\eta_i) + \frac{\partial}{\partial v} \mathfrak{J}_i(t,v|\eta_i) = 0, \tag{C2}$$

where the total probability flux is defined as

$$\mathcal{J}_i(t,v|\eta_i) = [\eta_i + v^2 + I_i(t)] p_i(t,v|\eta_i).$$

A boundary condition for the flux, consistent with the reset mechanism of the QIF model, is again imposed. The firing rate of the population $r_i(t)$ is the flux through the threshold, denoting again

$$r_i(t,\eta_i) = \lim_{v\to+\infty} \mathcal{J}_i(t,v|\eta_i);$$

the total firing rate is thus given by

$$r_i(t) = \int_{-\infty}^{+\infty} \mathcal{L}_i(\eta_i) r(t,\eta_i)\, d\eta_i,$$

where $\mathcal{L}_i$ the Lorentzian distribution,

$$\mathcal{L}_i(\eta_i) = \frac{1}{\pi} \frac{\Delta_i}{(\eta_i - \bar{\eta_i})^2 + \Delta_i^2},$$

that defines the probability that a randomly chosen I-cell has an intrinsic parameter η_i.

2. Reduction

Applying the reduction method (B1) to the two probability densities $p_e(t,v|\eta_e)$ and $p_i(t,v|\eta_i)$ will therefore lead to the reduced dynamical system:

$$\begin{aligned} \tau_e \frac{d}{dt} r_e &= \frac{\Delta_e}{\pi\tau_e} + 2\pi r_e V_e \\ \tau_e \frac{d}{dt} V_e &= V_e^2 + \bar{\eta}_e + I_e(t) - \pi^2 r_e^2, \end{aligned} \tag{C3}$$

and for the I cells

$$\begin{aligned} \tau_i \frac{d}{dt} r_i &= \frac{\Delta_i}{\pi\tau_i} + 2\pi r_i V_i \\ \tau_i \frac{d}{dt} V_i &= V_i^2 + \bar{\eta}_i + I_i(t) - \pi^2 r_i^2. \end{aligned} \tag{C4}$$

Assuming an instantaneous synaptic dynamic, the injected current at the soma of the excitatory cells $I_e(t)$ will be given by

$$I_e(t) = I_e^{\text{ext}}(t) + J_{ee}\tau_e r_e - J_{ei}\tau_e r_i,$$

respectively for the I cells,

$$I_i(t) = I_i^{\text{ext}}(t) + J_{ie}\tau_i r_e - J_{ii}\tau_i r_i,$$

where I^{ext} is an extern al current and J the synaptic strength.

APPENDIX D: PRC

1. PRC for a general system

Let us consider a general dynamical system,

$$\frac{d}{dt} x(t) = F[x(t)],$$

where $x \in \mathcal{R}^n$. Assume that the system admits a stable limit cycle $x_0(t)$, then if the system is perturbed by a small perturbation, the solution can be written as

$$x(t) = x_0(t) + \epsilon p(t),$$

where $p(t)$ is the perturbed part. Up to a linearization, we get that

$$\frac{d}{dt} p(t) = DF[x_0(t)] \cdot p(t).$$

The iPRC [8] is defined as

$$\frac{d}{dt}[Z(t)\cdot p(t)],$$

which is equivalent to

$$\begin{aligned} \frac{d}{dt}[Z(t)\cdot p(t)] &= \frac{d}{dt} Z(t)\cdot p(t) + Z(t)\cdot \frac{d}{dt} p(t) \\ &= \frac{d}{dt} Z(t)\cdot p(t) + Z(t)\cdot DF[x_0(t)]\cdot p(t) \\ &= \frac{d}{dt} Z(t)\cdot p(t) + DF[x_0(t)]^T \cdot Z(t)\cdot p(t) \\ &= \left\{ \frac{d}{dt} Z(t) + DF[x_0(t)]^T \cdot Z(t) \right\} \cdot p(t). \end{aligned}$$

Since the last equation is valid for every perturbation $p(t)$, we get that the iPRC is solution of the adjoint equation:

$$\frac{d}{dt} Z(t) = -DF[x_0(t)]^T \cdot Z(t).$$

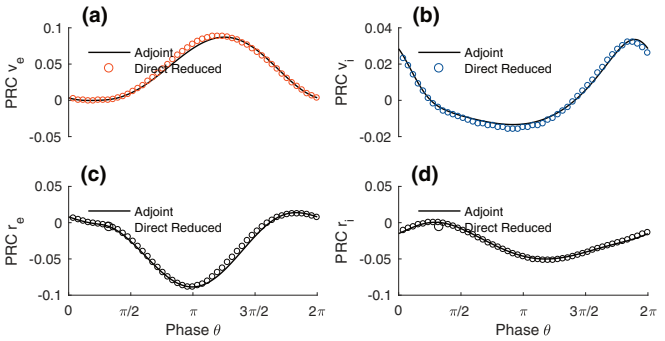

FIG. 6. Comparison between PRCs. The black line is obtained via the adjoint method, the dots are obtained via direct perturbation of the reduced system. (a) The perturbation is made with a square wave current pulse (amplitude 5, duration 0.05) on the V_e component. (b) The perturbation is made with a square wave current pulse (amplitude 5, duration 0.08) on the V_i component. (c) The perturbation is made with a square wave current pulse (amplitude 3, duration 0.03) on the r_e component. (d) The perturbation is made with a square wave current pulse (amplitude 2, duration 0.02) on the r_i component. Parameters are the same as in Fig. 1.

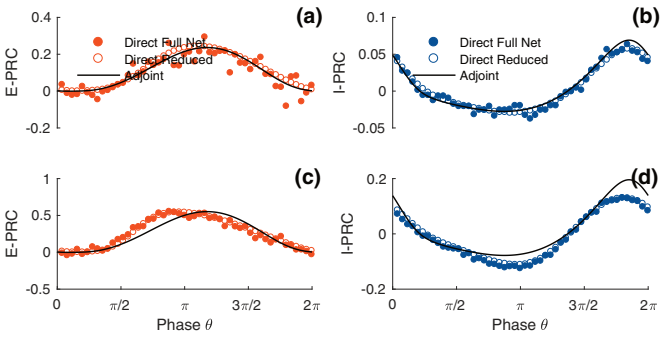

FIG. 7. Comparison between PRCs. The black line is obtained via the adjoint method, the dots are obtained via direct perturbation made either on the full network or on the reduced system. (a) The perturbation is made with a square wave current pulse (amplitude 8, duration 0.09) on the V_e component. (b) The perturbation is made with a square wave current pulse (amplitude 20, duration 0.09) on the V_i component. (c) The perturbation is made with a square wave current pulse (amplitude 5, duration 0.09) on the V_e component. (d) The perturbation is made with a square wave current pulse (amplitude 20, duration 0.09) on the V_i component. Parameters are the same as in Fig. 1.

2. PRC of the E-I system

We now assume that

$$O(t) = (r_{e_o}(t), V_{e_o}(t), r_{i_o}(t), V_{i_o}(t)),$$

is a stable limit cycle of the E-I system (C3)–(C4) of period T:

$$O(t) = O(t+T).$$

The iPRC $Z(t)$ is a periodic vector of four components,

$$Z(t) = (Z_{r_e}(t), Z_{v_e}(t), Z_{r_i}(t), Z_{v_i}(t)),$$

that is a solution of the adjoint equation

$$-\frac{d}{dt}Z(t) = \mathcal{M}(t)^T \cdot Z(t),$$

where the matrix $M(t)$ is given by a linearization of the E-I system (C3)–(C4) around the limit cycle:

$$\mathcal{M}(t) = \begin{bmatrix} 2V_{e_o}(t)/\tau_e & 2r_{e_o}(t)/\tau_e & 0 & 0 \\ -2\tau_e\pi^2 r_{e_o}(t) + J_{ee} & 2V_{e_o}(t)/\tau_e & -J_{ei} & 0 \\ 0 & 0 & 2V_{i_o}(t)/\tau_i & 2r_{i_o}(t)/\tau_i \\ J_{ie} & 0 & -2\tau_i\pi^2 r_{i_o}(t) - J_{ii} & 2V_{i_o}(t)/\tau_i \end{bmatrix}.$$

The $Z(t)$ is given by the unique periodic solution that satisfies the normalization condition

$$Z(t) \cdot \dot{O}(t) = \frac{2\pi}{T}.$$

The panels of Fig. 6 respectively compare the PRC obtained from perturbation of the reduced dynamical E-I system (C3)–(C4) with the four components of the iPRC $Z(t)$. When the perturbation is small enough, the iPRC $Z(t)$ will be proportional to the PRC. This is indeed what we observe in Fig. 6 for the different components of the PRC.

Although we obtained four components

$$Z(t) = (Z_{r_e}(t), Z_{v_e}(t), Z_{r_i}(t), Z_{v_i}(t));$$

in practice, only the voltage components are meaningful; see Figs. 6(a)–6(b). The reason is that, on the full spiking network, perturbation can be made only by a current that affects the membrane potential. The panels of Fig. 6 compare the PRC obtained from perturbation of the full spiking network, of the reduced dynamical system and the voltage components of the iPRC $Z(t)$. As expected, the network PRC is more noisy than the reduced system PRC; see Figs. 7(a)–7(b). When the strength of the perturbation is increased, we do observe a mismatch between the PRCs and the iPRC; see Figs. 7(c)–7(d).

[1] L. Glass and M. C. Mackey, *From Clocks to Chaos: The Rhythms of Life* (Princeton University Press, 1988).

[2] A. T. Winfree, *The Geometry of Biological Time* (Springer, New York, 2001).

[3] G. Buzsaki, *Rhythms of the Brain* (Oxford University Press, Oxford, 2006).
[4] P. Ashwin, S. Coombes, and R. Nicks, J. Math. Neurosci. **6**, 2 (2016).
[5] H. Nakao, Contemp. Phys. **57**, 188 (2016).
[6] K. M. Stiefel and G. B. Ermentrout, J. Neurophysiol. **116**, 2950 (2016).
[7] C. C. Canavier, Curr. Opinion Neurobiol. **31**, 206 (2015).
[8] E. Brown, J. Moehlis, and P. Holmes, Neural Comput. **16**, 673 (2004).
[9] Y. Kawamura, H. Nakao, and Y. Kuramoto, Phys. Rev. E **84**, 046211 (2011).
[10] Z. Levnajić and A. Pikovsky, Phys. Rev. E **82**, 056202 (2010).
[11] K. Kotani, I. Yamaguchi, L. Yoshida, Y. Jimbo, and G. B. Ermentrout, J. R. Soc. Interface **11** (2014).
[12] K. Kotani, I. Yamaguchi, Y. Ogawa, Y. Jimbo, H. Nakao, and G. B. Ermentrout, Phys. Rev. Lett. **109**, 044101 (2012).
[13] H. Nakao, T. Yanagita, and Y. Kawamura, Phys. Rev. X **4**, 021032 (2014).
[14] E. Montbrió, D. Pazó, and A. Roxin, Phys. Rev. X **5**, 021028 (2015).
[15] G. Deco, V. K. Jirsa, P. A. Robinson, M. Breakspear, and K. Friston, PLoS Comput. Biol. **4**, 1 (2008).
[16] E. Ott and T. M. Antonsen, Chaos **18**, 037113 (2008).
[17] T. B. Luke, E. Barreto, and P. So, Neural Comput. **25**, 3207 (2013).
[18] E. M. Izhikevich, in *Dynamical Systems in Neuroscience*, edited by T. Sejnowski and T. A. Poggio (MIT Press, Cambridge, MA, 2007).
[19] G. B. Ermentrout and D. Terman, *Mathematical Foundations of Neuroscience* (Springer, New York, 2010).
[20] H. R. Wilson and J. D. Cowan, Biophys. J. **12**, 1 (1972).
[21] M. Bartos, I. Vida, and P. Jonas, Nat. Rev. Neurosci. **8**, 45 (2007).
[22] R. M. Smeal, G. B. Ermentrout, and J. A. White, Phil. Trans. R. Soc. London B: Biol. Sci. **365**, 2407 (2010).
[23] G. B. Ermentrout, R. F. Galn, and N. N. Urban, Trends Neurosci. **31**, 428 (2008).
[24] D. Pazó and E. Montbrió, Phys. Rev. Lett. **116**, 238101 (2016).
[25] K. M. Hannay, V. Booth, and D. B. Forger, Phys. Rev. E **92**, 022923 (2015).
[26] J. A. Cardin, M. Carlen, K. Meletis, U. Knoblich, F. Zhang, K. Deisseroth, L.-H. Tsai, and C. I. Moore, Nature (London) **459**, 663 (2009).
[27] T. Akam, I. Oren, L. Mantoan, E. Ferenczi, and D. M. Kullmann, Nat. Neurosci. **15**, 763 (2012).
[28] E. Maris, P. Fries, and F. van Ede, Trends Neurosci. **39**, 86.
[29] R. T. Canolty and R. T. Knight, Trends Cognitive Sci. **14**, 506 (2010).